Geoscience Frontiers 6 (2015) 571–577

HOSTED BY

Contents lists available at ScienceDirect

China University of Geosciences (Beijing)

Geoscience Frontiers

journal homepage: www.elsevier.com/locate/gsf

Research paper

# $^{40}Ar/^{39}Ar$ ages of seamount trachytes from the South China Sea and implications for the evolution of the northwestern sub-basin

Xiaohu Li [a,b,*], Jiabiao Li [a,b], Xing Yu [a,b], Chunsheng Wang [b,c], Fred Jourdan [d]

[a] Key Laboratory of Submarine Geoscience, State Oceanic Administration, Hangzhou 310012, China
[b] Second Institution of Oceanography, State Oceanic Administration, Hangzhou 310012, China
[c] Key Laboratory of Marine Ecosystem and Biogeochemistry, State Oceanic Administration, Hangzhou 310012, China
[d] Western Australian Argon Isotope Facility, Department of Applied Geology and JdL Centre, Curtin University, GPO Box U1987, Perth 6845, WA, Australia

ARTICLE INFO

*Article history:*
Received 16 March 2014
Received in revised form
8 August 2014
Accepted 21 August 2014
Available online 16 September 2014

*Keywords:*
$^{40}Ar/^{39}Ar$ dating
Seamount trachyte
Northwest sub-basin
Expansion history
South China Sea

ABSTRACT

A chronological study of seamount rocks in the South China Sea basin provides a great opportunity to understand the expansion and evolution history of the sea basin. In this paper, we analyzed the $^{40}Ar/^{39}Ar$ age of trachytic samples collected from the Shuangfeng seamounts in the northwestern sub-basin of the South China Sea. The two samples yielded plateau ages of 23.80 ± 0.18 and 23.29 ± 0.22 Ma, respectively, which indicate magmatic activity in late Oligocene which helpful constraints the expansion time of the northwest sub-basin. Previous studies suggested that the northwestern sub-basin and southwestern sub-basin have experienced a relatively consistent expansion in the NW–SE direction followed by a late expansion of the eastern sub-basin. We concluded that the expansion of the northwestern sub-basin began prior to ca. 24 Ma, which also implicated magmatic events of a late or stop expansion of the northwestern sub-basin combined with our results of $^{40}Ar/^{39}Ar$ age data and previous geophysical data.



## 1. Introduction

The South China Sea is located at the junction of the Eurasia plate, western Pacific plate, and India-Australian plate and has experienced a complete process of continental rifting, seafloor spreading, and subduction. The South China Sea is a typical representative of western Pacific marginal seas. According to its water depth and seafloor topographic features, South China Sea is divided into three sub-basins, i.e., the northwestern, central, and southwestern sub-basins (Yao, 1996). The northwestern sub-basin contains the smallest area, and its expansion is in the NW–SE direction, similar to the expansion direction of the southwestern sub-basin. The border at longitude 116°E divides the South China Sea basin into two sub-basins, i.e., the eastern sub-basin and southwestern sub-basin. The expansion age and formation mechanism of the South China Sea are important to constrain in gaining an in-depth understanding of the continental marginal sea evolution and its interior geodynamic process and is an important aspect to "construct the history of life for the marginal sea" (Wang, 2012).

Presently, the study of the expansion history and mechanism of the South China Sea primarily depends on geophysical approaches, such as gravity, magnetic and seismic methods. In particular, tracking, analyzing, and comparing magnetic stripes are the most effective approach to determine the expansion age of a sea basin. Early work on the subject inferred that the seafloor expansion in the South China Sea began in early Eocene (~32 Ma) according to the magnetic anomaly bands and heat flow values. Along with its expansion and evolution, the ridge changed from an initial E–W direction to an NE–SW direction. Additionally, along with the variation in the expansion rate, there were at least four separate evolutionary stages; expansion eventually ended in the middle Miocene (~15.5 Ma) (Taylor and Hayes, 1983; Briais et al., 1993; Kido et al., 2001). However, because the magnetic anomaly band for the seafloor expansion in the South China Sea was identified more than 30 years ago (Taylor and Hayes, 1980, 1983), its use as evidence is controversial in the expansion history of the South China Sea. The main focus has been to determine the starting age of the three sub-basin expansions (Taylor and Hayes, 1980; Yao, 1996, 1997, 1998, 1999; Barckhausen and Roeser, 2004; Song and Li, 2012; Wei et al., 2012; Zhang et al., 2012) to determine the expansion

* Corresponding author. 36 Baochubei Road, Hangzhou 310012, China. Tel.: +86 0571 81061780 (office), +86 13738045385 (mobile).
*E-mail address:* lixh09@gmail.com (X. Li).
Peer-review under responsibility of China University of Geosciences (Beijing)

http://dx.doi.org/10.1016/j.gsf.2014.08.003

mechanism (Ding et al., 2002, 2009; Li et al., 2002, 2012; Li and Song, 2012; Yan et al., 2014). The limited number of geological and geophysical surveys, the complexity of geophysical data processing, and the inevitable multi-solution problem during interpretation are the primary reasons why there are considerable deviations in results and understanding. Therefore, if we can combine geochronological and geochemical approaches on well characterized rock samples to determine the age and composition of oceanic crusts and volcanic chain samples, we can more accurately determine the time of the opening and interior activity of the South China Sea basin (Xu et al., 2012).

Xu et al. (2012) believed that, according to the context relationship with the opening events of the South China Sea (32–15.5 Ma), the volcanic activity in the South China Sea and adjacent areas can be divided into three stages, i.e., before the opening of the South China Sea basin, during the opening period, and after the opening period. According to the current study, the Eocene volcanic rock was primarily produced in the northern margin of the South China Sea and in the coastal areas of South China before the South China Sea basin opened, similar to the bimodal volcanic rocks in the Sanshui, Lianping, and Heyuan Basin (Chung et al., 1997). The basalt rocks obtained in the eastern basin and seamount chain using the trawl consist primarily of alkaline basalts or the transition type between tholeiitic basalts and alkaline basalts (Taylor and Hayes, 1983). The measured basalt age is mostly less than 15.5 Ma (Tu et al., 1992; Yan et al., 2008; Wang et al., 2009), which is due to the magmatism after the expansion period of the South China Sea. Several pieces of MORB-like basalt samples were obtained in the southwestern sub-basin; their K-Ar age is approximately 11.5–3.4 Ma (Han, 2011). This result contributes to a new understanding of the expansion history of the southwestern sub-basin.

For the basalt samples acquired in the South China Sea basin, there are no reports on rock samples in the northwestern sub-basin. There are also no reports on the age data and lithology of basalts during the opening period. In this paper, we report on the Ar-Ar age of rock samples obtained in the Shuangfeng seamounts of the northwestern sub-basin in the South China Sea and combine the results of previous studies to further investigate the expansion and evolution history of the northwestern sub-basin in the South China Sea.

## 2. Regional geological background of the northwestern sub-basin

The northwestern sub-basin is northwest of the central abyssal plain in the South China Sea (Fig. 1). The Zhongsha Islands are located to its south, and the Xisha Islands are located to its west; the NE-trending Zhongsha trough is located on the southwestern continental margin, and the EW-trending Xisha trough is located on the western continental margin. The northern continental margin of the South China Sea is to its north, and the NW-trending sea valley outside the Pearl River estuary extends from the margin of the continental shelf to the northwestern sea basin, which forms a continental rise on the margin of the sea basin. The sea basin is located in the NE–SW direction, and its shape is similar to a rhombus. The seafloor gradually tilts from the SW to NE, and the water depth is between 3000 and 3800 m. The NE-trending Shuangfeng seamounts are distributed in the middle of the basin. The lowest water depth on the top is 2407 m, and the largest height difference relative to the seafloor is greater than 1100 m (Yao, 1999; Ding et al., 2009).

The free-air gravity anomaly of the northwestern sub-basin is generally in the NE direction and exhibits a low-high-low trend from north to south. The central area of the high anomaly corresponds to Shuangfeng seamounts, and the high-density substance in the central basin is likely closely related to cracks in the crust or the invasion of high-density substances from the mantle (Ding et al., 2002).

The geomagnetic anomaly of the northwestern sub-basin has the consistent trend related to the gravity anomaly and also exhibits an NE–NEE trending. The geomagnetic anomaly is roughly distributed in bands, with a relatively short wavelength and an amplitude approximately between 50 and 150 nT. Four magnetic anomaly zones can be divided from north to south. The banded magnetic anomaly with interlaced positive and negative polarity shows the expansion nature of the seafloor, whereas the morphology is relatively vague (Ding et al., 2009).

The seismic line analysis indicates that the northwestern sub-basin consists primarily of sediment in Neogene and Paleogene sediment is relatively thin. Three sets of seismic reflection layers are identified in the Cenozoic sediments of the sea basin, and the stratigraphic ages from top to bottom are middle Miocene–Quaternary (layer group I), early Miocene (layer group II), and Paleogene (primarily Oligocene, layer group III) (Ding et al., 2009) .

## 3. Samples and analysis methods

The samples used in this study were collected from Shuangfeng seamounts (115°07′02″E, 18°17′59″N) in the South China Sea (Fig. 1). Shallow drilling was performed to acquire the core samples from the bottom of the seamounts, and there was an approximately 0.5-cm thick Fe-Mn oxide layer at the top of the rock cores. The lower part of the rocks has a porphyritic structure in the blocks, which is named trachyte. The images of the rock core slicers (Fig. 2) and microscopic crossed nicols (Fig. 3) are as follows.

Sample S09-1 (Fig. 2A) is relatively fresh with a porphyritic structure with plagioclase phenocrysts and a small amount of pyroxene and olivine phenocrysts (Fig. 3A). Plagioclase has twins with relatively wide stripes and is partial basic plagioclase with a long axis of approximately 0.5 mm. The substrate has an intergranular-intersertal structure, and the distribution of the long stripe plagioclase grids are filled with pyroxene and serpentinization of olivine microcrystalline and volcanic glass. Sample S09-2 (Fig. 2B) is also relatively fresh with a porphyritic structure, and the phenocrysts are olivine, pyroxene, and plagioclase (Fig. 3B). The edge of the olivine is iddingsite and is a reddish brown color in single, polarized light. The plagioclase phenocrysts can reach up to 1 mm in size with the development of albite twins, and the edge displays signs of corrosion. The substrate has an intergranular-intersertal structure. The long axis of the long, thin stripe or plate plagioclase in the substrate can reach up to 0.3 mm in size with a random distribution and orientation. Its structure is porous with a porosity of approximately 5%.

We selected 2 fresh samples from Shuangfeng seamount in the northwestern sub-basin of the South China Sea for $^{40}Ar/^{39}Ar$ dating and separated unaltered, optically transparent, 150–215 microns grain of groundmass. Samples were loaded into 2 large wells of one 1.9 cm diameter and 0.3 cm depth aluminum disc. These wells were bracketed by small wells that included Fish Canyon sanidine (FCs) used as a neutron fluence monitor for which an age of 28.294 ± 0.036 Ma ($1\sigma$) was adopted (Renne et al., 2011). The discs were Cd-shielded (to minimize undesirable nuclear interference reactions) and irradiated for 2 h in the Hamilton McMaster University nuclear reactor (Canada) in position 5C (Samples S09-1 and S09-2) and 3 h in the USGS TRIGA reactor, in Denver (USA). The mean J-values computed from standard grains within the small pits and determined as the average and standard deviation of J-values of the small wells for each irradiation disc is given along with the raw data in Annex S09-1 and Annex S09-2. Mass discrimination is given

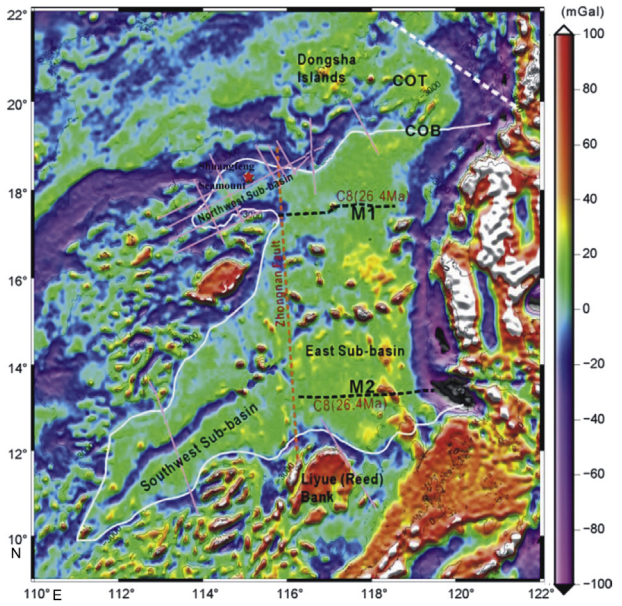


**Fig. 1.** Free-air gravity anomaly map of the South China Sea (based on the 1-min grid) (Modified after Li and Song, 2012). The red solid pentacle in the Shuangfeng Seamount marks the sampling site of the rocks. M1 and M2 are major magnetic boundaries in the East sub-basin, and their ages are estimated to be C8 (~26 Ma). The white solid line marks the continent-ocean boundary (COB). The light red dashed line marks the Zhongnan Fault. The white bold dashedline marks the Luzon-Ryukyu Transform Boundary.

in Annex for each sample and was monitored using an automated air pipette and calculated relative to an air ratio of 298.56 ± 0.31 (Lee et al., 2006). The correction factors for interfering isotopes were $(^{39}Ar/^{37}Ar)_{CA} = 7.30 \times 10^{-4}$ (±11%), $(^{36}Ar/^{37}Ar)_{CA} = 2.82 \times 10^{-4}$ (±1%) and $(^{40}Ar/^{39}Ar)_K = 6.76 \times 10^{-4}$ (±32%) for McMaster reactor and $(^{39}Ar/^{37}Ar)_{CA} = 7.06 \times 10^{-4}$ (±7%), $(^{36}Ar/^{37}Ar)_{CA} = 2.81 \times 10^{-4}$ (±3%) and $(^{40}Ar/^{39}Ar)_K = 6.76 \times 10^{-4}$ (±10%) (Cosca et al., 2011) for the USGS TRIGA reactor.

The $^{40}Ar/^{39}Ar$ analyses were performed at the western Australian Argon Isotope Facility at Curtin University. The sample was step-heated in a double vacuum high frequency Pond Engineering© furnace. The gas was purified in a stainless steel extraction line using two AP10 and one GP50 SAES getters and a liquid nitrogen condensation trap. Ar isotopes were measured in static mode using a MAP 215-50 mass spectrometer (resolution of ~400; sensitivity of $4 \times 10^{-14}$ mol/V) with a Balzers SEV 217 electron multiplier mostly using 9 to 10 cycles of peak-hopping.

The data acquisition was performed with the Argus program written by M.O. McWilliams and ran under a LabView environment. The raw data were processed using the ArArCALC software (Koppers, 2002) and the ages have been calculated using the decay constants recommended by Renne et al. (2010). Blanks were monitored every 3 to 4 steps and typical $^{40}Ar$ blanks range from $1 \times 10^{-16}$ to $2 \times 10^{-16}$ mol. Ar isotopic data corrected for blank, mass discrimination and radioactive decay are given in Annex S09-1 and Annex S09-2. Individual errors are given at the $1\sigma$ level. Our criteria for the determination of plateau are as follows: plateaus must include at least 70% of $^{39}Ar$. The plateau should be distributed over a minimum of 3 consecutive steps agreeing at 95% confidence level and satisfying a probability of fit ($P$) of at least 0.05. Plateau ages (Figs. 4 and 5) are given at the $2\sigma$ level and are calculated using the mean of all the plateau steps, each weighted by the inverse variance of their individual analytical error. Mini-plateaus are defined similarly except that they include between 50% and 70% of $^{39}Ar$. Integrated ages ($2\sigma$) are calculated using the total gas released for each Ar isotope. Inverse isochrons include the maximum number of steps with a probability of fit ≥0.05. S-factors showing the spread along the inverse isochron (Jourdan and Renne, 2007) and $^{40}Ar/^{36}Ar$ intercept values are provided. All sources of uncertainties are included in the calculation.

## 4. Results

The results of the $^{40}Ar/^{39}Ar$ analysis using the step-heating method for the seamount trachyte in the northwestern sub-basin are shown in Table 1, and the corresponding plateau age and inverse isochron age are shown in Figs. 4 and 5, respectively. Sample S09-1 yielded a well-defined $^{40}Ar/^{39}Ar$ plateau age of 23.80 ± 0.18 Ma ($2\sigma$) (e.g. Fig. 4A) with an inverse isochron age of 23.81 ± 0.14 Ma (e.g. Fig. 4B) and $^{40}Ar/^{36}Ar$ initial value of 295 ± 34 (MSWD = 1.20). The same result of sample S09-2 also yielded a well-defined $^{40}Ar/^{39}Ar$ plateau age of 23.29 ± 0.22 Ma ($2\sigma$) (e.g. Fig. 5A) with an inverse isochron age of 23.29 ± 0.20 Ma (e.g. Fig. 5B) and $^{40}Ar/^{36}Ar$ initial value of 301 ± 62 Ma (MSWD = 0.76). The plateau ages obtained by the two rocks (e.g. Figs. 4 and 5) are concordant with each other within the error range. We interpret these two ages are indicating the age of the eruptions of the rocks.

## 5. Discussions

For the northwestern sub-basin, because the sea basin is narrow, it is difficult to compare the magnetic anomaly bands, and there is considerable disagreement between the expansion age and manner of the sea basin. Briais et al. (1993) found that the expansion of the South China Sea basin began at 32 Ma (No. 11 magnetic anomaly), and the oceanic ridge transited to the south at 26–24 Ma (7 and 6b magnetic anomaly). Then, the South China Sea basin rapidly extended in the SW direction, which caused a dramatic change in the morphology of the basin. Using seismic survey lines, Yao (1999)

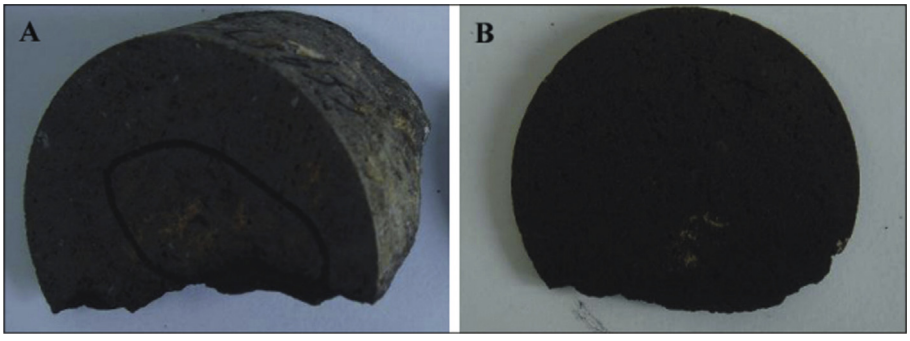


**Fig. 2.** Core samples S09-1 (A) and S09-2 (B) from the northwest sub-basin in the South China Sea.

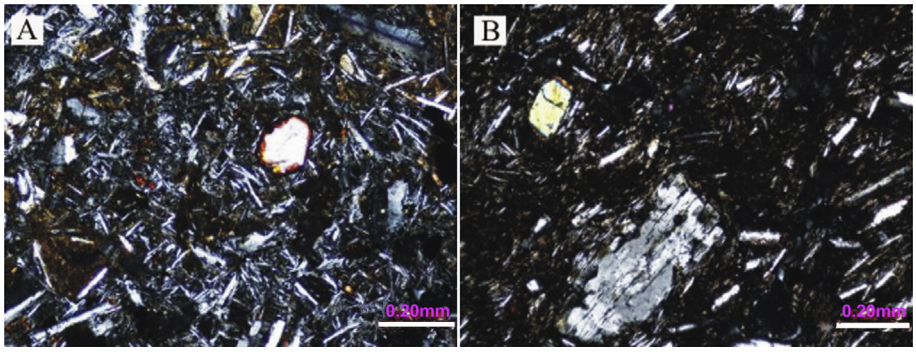


**Fig. 3.** Microscopic images of thin-sections of samples S09-1 (A) and S09-2 (B) (crossed nicols).

found that the substrate of the northwestern sub-basin has an additional set of low-frequency intermittent reflections relative to the central sub-basin, which indicates that the formation of the northwestern sub-basin occurred earlier than the formation of the central sea basin, where the structural trending is similar to the southwestern sub-basin. It is inferred that the northwestern sub-basin and the southwestern sub-basin were formed during the same seafloor expansion at a formation time of 42–35 Ma. By interpreting three seismic survey lines and one deep reflection seismic profile through the northwestern sub-basin, Ding et al. (2009) concluded that the northwestern sub-basin is a sea basin that began to develop at 30 Ma. After 25 Ma, the expansion shaft of the South China Sea transited to the south, and the southwestern sub-basin began to expand. In particular, the NW-trending compressive stress on the Zhongsha-Xisha block caused the northwestern sub-basin to cease activity and entered the stage of thermodynamic deposition. Wei et al. (2012) used the features of passive overlying of sedimentary strata and gravity and magnetic anomalies of the basement to infer that the initial expansion time of the northwestern sub-basin in the South China Sea was in early Oligocene and that expansion ended at the early period of late Oligocene. The developmental time of the sea basin was short. The most recently collected, high-density (space of survey lines less than 10 km), ship-measured geomagnetic data clearly shows the presence of magnetic strips in the northwestern sub-basin. With the constraints imposed from OBS and multi-channel seismic data, we infer that the primary expansion of the northwestern sub-basin began at 35.8 Ma and that expansion eventually ended at 33.2 Ma (Zhang et al., 2012). Presently, because there are no reports on the petrology of the northwestern sub-basin, there is a lack of additional constraints to determine the expansion time of the sea basin.

According to the existing understanding of the expansion age of the northwestern sub-basin, the expansion age spans from late Eocene to Oligocene. There is a considerable deviation in the starting age of the sea basin expansion, which also affects the inference of the expansion history of the entire South China Sea basin. In this paper, we determined the formation age of rocks to be 23–24 Ma by measuring the Ar-Ar age of the trachyte of the NE-trending Shuangfeng seamounts in the northwestern sub-basin, which represents the time of magmatism that occurred during the expansion of the sea basin. Along with the results of previous studies (Taylor and Hayes, 1983; Briais et al., 1993; Barckhausen and Roeser, 2004; Ding et al., 2009; Li et al., 2012; Song and Li, 2012), we suggest that this age illustrates a period of magmatic activity occurring after the northwestern sub-basin began to expand and therefore, narrows down the age of the onset of the expansion of the northwestern sub-basin. This is consistent with our current understanding of the timing of the expansion of the eastern sub-basin. However, the timing of the expansion of the northwestern sub-basin is significantly different from the timing observed for the southwestern sub-basin. This comparison is further discussed in this paper.

Taylor and Hayes (1983) speculated that the reasonable expansion direction of the southwestern sub-basin is between the NW–SE direction (perpendicular to the inferred direction of the residual expansion center) and the N–S direction (parallel to the expansion direction to the east of 116°E). Subsequent studies that investigated the multi-beam and magnetic survey line found that

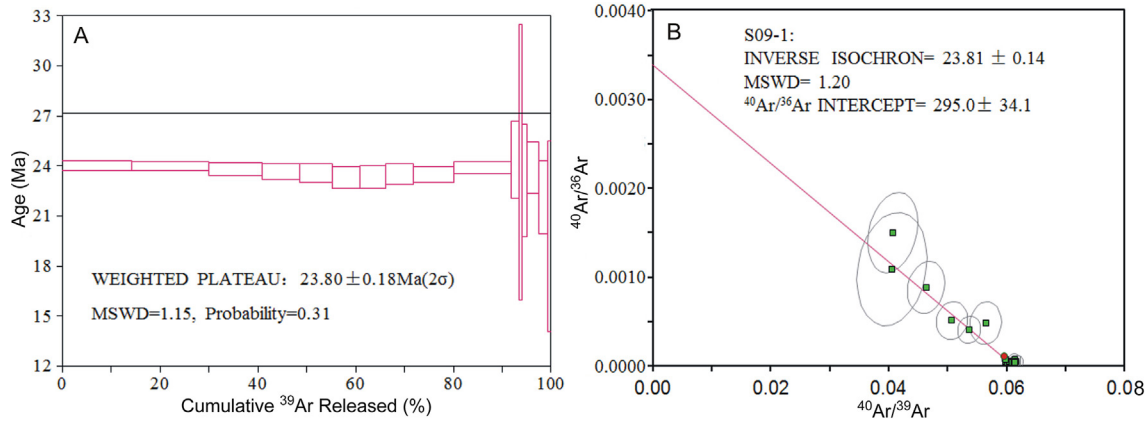


**Fig. 4.** $^{40}$Ar/$^{39}$Ar age spectrum (A) and inverse isochron (B) of sample S09-1.

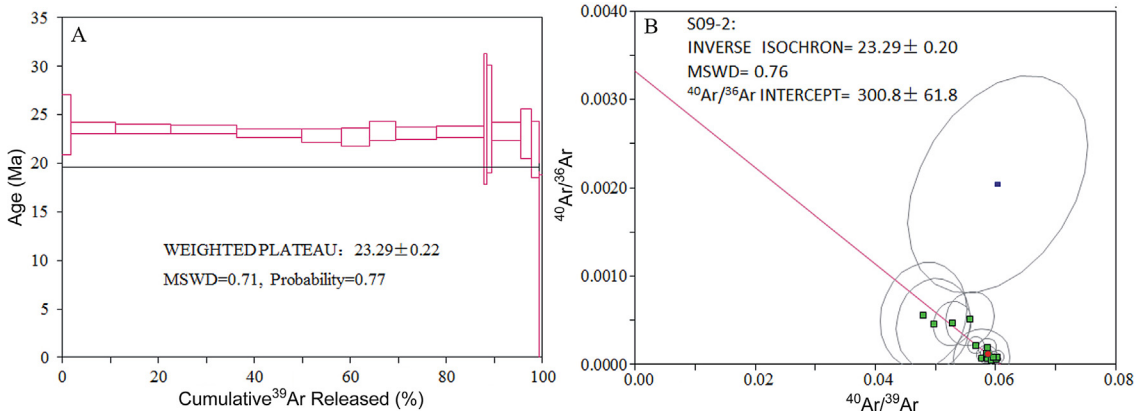


**Fig. 5.** $^{40}Ar/^{39}Ar$ age spectrum (A) and inverse isochron (B) of sample S09-2.

the late expansion time of the eastern sea basin once turned from the original near NS direction to the near NW–SE direction, which is similar to the expansion direction (NW–SE) of the southwestern sub-basin. At approximately 21 Ma (No. 6a), there was an accelerated expansion event in the eastern sea basin, which also confirms that the southwestern sub-basin and the eastern sub-basin experienced seafloor expansion in the same direction as Miocene (Li et al., 2002). Recently, the re-analysis of the magnetic anomaly zones in the South China Sea basin showed that in the eastern sub-basin, the expansion direction slightly changed from the near NS trending to NNW–SSE trending after the magnetic anomaly C6a (~21 Ma); the expansion direction of the southwestern sub-basin has always been NW–SE trending, and there have been no significant changes in the expansion direction in the course of expansion (Li and Song, 2012). Yao (1999) also found that the southwestern sub-basin and the northwestern sub-basin have a similar structural trend. Although their understanding of the expansion time is different from others, these authors believed that the southwestern sub-basin and the northwestern sub-basin were formed during the same seafloor expansion.

From the perspective of expansion age and oceanic ridge transition, the magnetic data acquired by the survey voyage of Sonne from Germany indicate that at approximately 31 Ma, the central South China Sea basin expanded in the N–S direction. At 25 Ma, the oceanic ridge transited southward by approximately 50 km, and the expansion rate increased significantly (the total expansion rate reached up to 7.3 cm/a). At the same time or within an extremely short time after the second expansion center, the southwestern

**Table 1**
$^{40}Ar/^{39}Ar$ stepwise heating analytical data for samples from the northwest sub-basin.

| Heating stages | | $^{40}Ar/^{39}Ar$ | $^{36}Ar/^{39}Ar$ | $^{37}Ar/^{39}Ar$ | Age (Ma) $\pm 2\sigma$ | $^{40}Ar(r)$ (%) | $^{39}Ar$ (%) | K/Ca $\pm 2\sigma$ |
|---|---|---|---|---|---|---|---|---|
| Sample S09-1, $J = 0.00081500 \pm 0.00000204$ | | | | | | | | |
| 1 | 550 °C | 16.7 | 0 | 0.04 | 24.02 ± 0.29 | 98.61 | 14.23 | 9.87 ± 19.61 |
| 2 | 600 °C | 16.64 | 0 | 0.08 | 23.98 ± 0.26 | 98.77 | 15.66 | 5.53 ± 4.63 |
| 3 | 650 °C | 16.56 | 0 | 0.03 | 23.81 ± 0.37 | 98.57 | 11 | 13.62 ± 47.52 |
| 4 | 700 °C | 16.42 | 0 | 0.06 | 23.66 ± 0.49 | 98.72 | 7.78 | 7.06 ± 16.32 |
| 5 | 750 °C | 16.34 | 0 | 0.04 | 23.56 ± 0.56 | 98.83 | 6.51 | 11.38 ± 52.47 |
| 6 | 800 °C | 16.31 | 0 | 0.06 | 23.32 ± 0.66 | 97.99 | 5.63 | 7.43 ± 27.79 |
| 7 | 850 °C | 16.23 | 0 | 0.09 | 23.35 ± 0.68 | 98.59 | 5.29 | 4.66 ± 11.03 |
| 8 | 900 °C | 16.3 | 0 | 0.12 | 23.51 ± 0.61 | 98.85 | 5.68 | 3.55 ± 5.85 |
| 9 | 950 °C | 16.28 | 0 | 0.2 | 23.49 ± 0.45 | 98.88 | 8.34 | 2.14 ± 1.13 |
| 10 | 1000 °C | 16.73 | 0 | 0.34 | 23.91 ± 0.34 | 97.95 | 11.79 | 1.25 ± 0.38 |
| 11 | 1050 °C | 19.7 | 0.01 | 0.54 | 24.37 ± 2.32 | 84.75 | 1.58 | 0.80 ± 1.35 |
| 12 | 1100 °C | 24.66 | 0.03 | 0.08 | 24.23 ± 8.24 | 67.37 | 0.45 | 5.39 ± 150.40 |
| 13 | 1150 °C | 21.57 | 0.02 | 0.17 | 23.15 ± 3.38 | 73.55 | 1.08 | 2.54 ± 19.56 |
| 14 | 1200 °C | 18.63 | 0.01 | 0.15 | 23.88 ± 1.54 | 87.84 | 2.48 | 2.78 ± 7.40 |
| 15 | 1300 °C | 17.71 | 0.01 | 0.48 | 22.15 ± 2.19 | 85.67 | 1.84 | 0.89 ± 1.19 |
| 16 | 1400 °C | 24.57 | 0.04 | 0.2 | 19.8 ± 5.71 | 55.17 | 0.65 | 2.19 ± 20.31 |
| Sample S09-2, $J = 0.00078900 \pm 0.00000197$ | | | | | | | | |
| 1 | 550 °C | 16.96 | 0 | 0.08 | 23.96 ± 3.12 | 97.82 | 1.66 | 5.30 ± 67.23 |
| 2 | 600 °C | 16.73 | 0 | 0.03 | 23.63 ± 0.60 | 97.85 | 9.42 | 15.56 ± 89.98 |
| 3 | 650 °C | 16.68 | 0 | 0.17 | 23.57 ± 0.49 | 97.78 | 11.57 | 2.51 ± 2.03 |
| 4 | 700 °C | 16.63 | 0 | 0.11 | 23.49 ± 0.43 | 98.47 | 13.74 | 4.03 ± 4.08 |
| 5 | 750 °C | 16.35 | 0 | 0.12 | 23.10 ± 0.43 | 98.18 | 13.5 | 3.65 ± 3.83 |
| 6 | 800 °C | 16.16 | 0 | 0.26 | 22.84 ± 0.70 | 97.43 | 8.3 | 1.65 ± 1.12 |
| 7 | 850 °C | 16.08 | 0 | 0.36 | 22.72 ± 0.94 | 94.27 | 5.77 | 1.18 ± 0.91 |
| 8 | 900 °C | 16.51 | 0 | 0.37 | 23.32 ± 0.97 | 96.52 | 5.57 | 1.18 ± 1.01 |
| 9 | 950 °C | 16.35 | 0 | 0.16 | 23.10 ± 0.65 | 97.5 | 8.47 | 2.69 ± 3.35 |
| 10 | 1000 °C | 16.44 | 0 | 0.4 | 23.22 ± 0.61 | 96.1 | 9.74 | 1.08 ± 0.46 |
| 11 | 1050 °C | 17.41 | 0.01 | 0.11 | 24.58 ± 6.75 | 83.49 | 0.77 | 4.07 ± 76.65 |
| 12 | 1100 °C | 17.41 | 0.01 | 1.33 | 24.58 ± 65.56 | 86.41 | 0.95 | 0.32 ± 0.49 |
| 13 | 1150 °C | 16.49 | 0 | 0.55 | 23.29 ± 0.91 | 93.46 | 6.05 | 0.79 ± 0.33 |
| 14 | 1200 °C | 16.34 | 0.01 | 0.11 | 23.08 ± 2.55 | 86.15 | 2.12 | 4.03 ± 30.76 |
| 15 | 1300 °C | 15.17 | 0.01 | 0.56 | 21.44 ± 2.91 | 84.5 | 1.8 | 0.77 ± 1.16 |

sub-basin began to expand, and the expansion ended at 20.5 Ma (Barckhausen and Roeser, 2004). What is different is that the oceanic ridge transited southward between 26 and 24 Ma (No. 7 and 6b anomaly) and then rapidly extended southwestward (Briais et al., 1993). At 20.5 Ma (No. 6 magnetic anomaly), the oceanic ridge then rapidly extended in southwest direction, and reached the largest extension of oceanic ridge. Li et al. (2012) suggested that the eastern sub-basin confined by the magnetic anomalies, M1 and M2, in the South China Sea basin (area D of the magnetic anomaly) must have had at least two transitions to reasonably explain why the average expansion rate of the oceanic crusts on the two sides of M1 to the north of the residual mid-oceanic ridge occurred more rapidly than the corresponding parts in the south. This result is consistent to some extent with the recent finding that the oceanic crust transition occurred at approximately 25 and 21 Ma. Ding et al. (2009) also found that the northwestern sub-basin began to develop at approximately 30 Ma, and the expansion shaft transited southward after 25 Ma. The expansion of the northwestern sub-basin ended and entered the post-crack deposition stage. Most recently, the new comparison and analysis were implemented for the critical survey lines of the magnetic anomaly in the eastern and southwestern sub-basin in the South China Sea, which further confirms that the expansion age of the eastern sub-basin is between 32 and 16.5 Ma (Song and Li, 2012). At approximately 26 Ma, strong magmatic activity might have occurred. There is still a considerable uncertainty in the possible expansion age of the southwestern sub-basin, which could be from 42 to 33 or 24–16 Ma. However, using the model with an expansion age of 24–16 Ma results in relatively good fitting results (Song and Li, 2012). In addition, the average heat flow data also indicate that the eastern sub-basin and southwestern sub-basin ($108 \pm 13$ m $Wm^{-2}$) are consistent with the early Miocene oceanic crust, which indicates that there is no considerable difference between the ages of the two sub-basins (Taylor and Hayes, 1983).

From the perspective of the expansion mechanism, we analyzed high-resolution, multi-beam tectonic topography of the southwestern sub-basin in the South China Sea and performed a comprehensive comparison study of the multi-channel seismic cross-sections (Li et al., 2002). In addition to identifying the magnetic strip anomaly, it is suggested that the southwestern sub-basin gradually expanded by progressing step by step from northeast to southwest, where the expansion age transitions from older to younger from the northeast to the southwest (Li et al., 2002). The introduction of the Zhongnan fracture explains the magnetic anomaly difference and the relative movement between the northwestern sub-basin (zone C2 of the magnetic anomaly) and north of the eastern sub-basin (zone C1 of magnetic anomaly). It is speculated that the volcanic rocks to the south of the northwestern sub-basin (zone C2 of magnetic anomaly) and the basalts causing the M1 magnetic anomaly (corresponding to the C8 magnetic anomaly at the age of 26 Ma) were likely formed at the same time of the seafloor expansion (Li and Song, 2012). In addition, for the significant tectonic deposition event at approximately 25 Ma, which was revealed by the stratigraphic record in 1999 at station 1148 of Ocean Drilling in the South China Sea (Li et al., 2006), Li and Song (2012) also speculated that it was linked to the formation of the M1 (C8) magnetic anomaly.

Based on the petrologic and geochemical studies, Cenozoic volcanic rocks are distributed in the South China Sea basin and adjacent areas (such as the Hainan Island, Leizhou-Qiongzhou area, Pear River Estuary basin, Indochina, and Reed Tablemount) (Wang et al., 1984; Kudrass et al., 1986; Zhu and Wang, 1989; Pautot et al., 1990; Li et al., 1991; Flower et al., 1992; Tu et al., 1992; Li and Liang, 1994; Zou et al., 1995; Xiao et al., 2006; Yan et al., 2008; Wang et al., 2009; Han, 2011; Yang et al., 2011). The lithology ranges from mafic to felsic rocks, and the rock type gradually changes from early bimodal volcanic rocks to the majority being alkaline basalts. The rock cores acquired from the Shuangfeng seamounts in the northwestern sub-basin are mainly trachyte. Such a conclusion was also reached by previous studies for other alkaline basalts that erupted during late Miocene in the South China Sea basin exhibit the OIB feature (Yan et al., 2008; Wang et al., 2009; Yang et al., 2011). The age of the seamounts in South China Sea basin generally becomes gradually younger going from north to south, and the rock age of the Shuangfeng seamounts is apparently older than the northernmost peak seamount ($19 \pm 5$ Ma; Li et al., 1991) although still within analytical due to the large uncertainties on the northernmost peak seamount. Our result indicates that there were older magmatism events in the northwestern sub-basin relative to the eastern sub-basin. In addition, from the features of tectonic and magmatic evolution on the active Cenozoic continental margin throughout the east part of China (Hu et al., 1994), the eruption of basalts on the continent reached a climax in the middle of Eocene (45–55 Ma, such as 51 Ma for Sanshui in Guangdong, and 49.6 Ma for Nanhai County). The convergence between the Eurasian plate and Pacific plate were in a relatively quiet period at approximately 30–40 Ma, and the basalt magma activity on the active continental margin east of Asia was low. Since Miocene (25 Ma), the basalt magma related to the rift environment in North China, Northeast China, and the southeast coastal area of China widely erupted, which persisted until Pliocene to Quaternary. The formation of the Shuangfeng seamounts in the northwestern sub-basin could also be related to the large-scale magmatism since 25 Ma on the active continental margin east of Asia, which was also somewhat coincident with the oceanic ridge transition, tectonic sedimentary events, and magmatism at approximately 25 Ma in the South China Sea basin.

## 6. Conclusions

We obtained two $^{40}Ar/^{39}Ar$ plateau ages of $23.80 \pm 0.18$ Ma and $23.29 \pm 0.22$ Ma ($2\sigma$) for two seamount trachyte samples in the northwest sub-basin. This indicates that magmatic activity occurred late in Oligocene. We concluded that the expansion of the northwestern sub-basin began prior to ca. 24 Ma, which also implicated magmatic events of a late or stop expansion of the northwestern sub-basin combined with our results of $^{40}Ar/^{39}Ar$ age data and previous geophysical data.

## Acknowledgments

This paper also benefits from discussions and supports from Dr. Aiguo Ruan, Weiwei Ding, Tao Zhao, Zhengli Wu in Second Institution of Oceanography, SOA and Dr. Chao Liu in Yale University. We would like to thank Dr. Inna Safonova for constructive comments that significantly improve the paper. This research was supported by the National Natural Science Foundation of China (Grant Nos. 91028006 and 41276055), the National Basic Research and Development Program (Grant Nos. 2007CB411700, 2013CB429700) and China Ocean Mineral R&D Association (COMRA) project (DY125-12-R-02, 04, 06).

## Appendix A. Supplementary data

Supplementary data related to this article can be found at http://dx.doi.org/10.1016/j.gsf.2014.08.003.

## References


Barckhausen, U., Roeser, H.A., 2004. Seafloor spreading anomalies in the South China Sea revisited. Geophysical Monograph Series 149, 121–125.

Briais, A., Patriat, P., Tapponnier, P., 1993. Updated interpretation of magnetic anomalies and seafloor spreading stages in the South China Sea:Implications for the Tertiary tectonics of Southeast Asia. Journal of Geophysical Research: Solid Earth (1978–2012) 98 (B4), 6299–6328.

Chung, S.L., Cheng, H., Jahn, B., O'Reilly, S.Y., Bingquan, Z., 1997. Major and trace element, and Sr-Nd isotope constraints on the origin of Paleogene volcanism in South China prior to the South China Sea opening. Lithos 40 (2), 203–220.

Cosca, M., Stunitz, H., Bourgeix, A.L., Lee, J.P., 2011. $^{40}Ar^{*}$ loss in experimentally deformed muscovite and biotite with implications for $^{40}Ar/^{39}Ar$ geochronology of naturally deformed rocks. Geochimica et Cosmochimica Acta 75 (24), 7759–7778.

Ding, W.W., Chen, H.L., Yang, S.F., Chu, F.Y., 2002. Geological and geophysical analysis of the Southwestern and Eastern Sub-Basins, South China Sea. Geological Journal of China Universities 8 (3), 268–279 (in Chinese with English abstract).

Ding, W.W., Li, M.B., Zhao, L.H., Ruan, A.G., Wu, Z.L., 2009. Cenozoic tectono-sedimentary characteristics and extension model of the Northwest Sub-basin, South China Sea. Earth Science Frontiers 16 (4), 147–156 (in Chinese with English abstract).

Flower, M.F., Zhang, M., Chen, C.Y., Tu, K., Xie, G.H., 1992. Magmatism in the south China basin: 2. Post-spreading Quaternary basalts from Hainan Island, south China. Chemical Geology 97 (1), 65–87.

Han, X.Q., 2011. The basalt of Southwest sub-basin in the South China Sea:evicence from petro-chemistry and chronology of the seafloor spreading. In: The Academic Workshop and Kick-off Meeting of the Major Research Program "Deep Sea Processes and Evolution of the South China Sea", 26–27 (in Chinese with English abstract).

Hu, S.X., Zhao, Y.Y., Hu, Z.H., Guo, J.C., Xu, B., 1994. Evolution and development of tectonics and magmatism at the active continental margin of the East China during Mesozoic and Cenozoic. Acta Petrologica Sinica 10 (4), 370–381.

Jourdan, F., Renne, P.R., 2007. Age calibration of the Fish Canyon sanidine $^{40}Ar/^{39}Ar$ dating standard using primary K-Ar standards. Geochimica et Cosmochimica Acta 71 (2), 387–402.

Kido, Y., Suyehiro, K., Kinoshita, H., 2001. Rifting to spreading process along the northern continental margin of the South China Sea. Marine Geophysics Research 22 (1), 1–15.

Koppers, A.A.P., 2002. ArArCALC-software for $^{40}Ar/^{39}Ar$ age calculations. Computers and Geosciences 28 (5), 605–619.

Kudrass, H.R., Wiedicke, M., Cepek, P., Kreuzer, H., Muller, P., 1986. Mesozoic and Cainozoic rocks dredged from the South China Sea (Reed Bank area) and Sulu Sea and their significance for plate-tectonic reconstructions. Marine and Petroleum Geology 3 (1), 19–30.

Lee, J.-Y., Marti, K., Severinghaus, J.P., Kawamura, K., Yoo, H.-S., Lee, J.B., Kim, J.S., 2006. A redetermination of the isotopic abundance of atmospheric Ar. Geochimica et Cosmochimica Acta 70 (17), 4507–4512.

Li, C.F., Song, T.R., 2012. Magnetic recording of the Cenozoic oceanic crustal accretion and evolution of the South China Sea basin. Chinese Science Bulletin 57 (20), 1879–1895.

Li, J.B., Ding, W.W., Wu, Z.Y., Zhang, J., Dong, C.Z., 2012. The propagation of seafloor spreading in the southwestern subbasin, South China Sea. Chinese Science Bulletin 57 (20), 1896–1905.

Li, J.B., Jin, X.L., Gao, J.Y., 2002. Research on the tectonic and swath bathymetry of east basin during the later seafloor spreading in the South China Sea. Science in China (Series D) 32 (3), 239–248.

Li, Q., Wang, P., Zhao, Q., Shao, L., Zhong, G.F., Tian, J., Cheng, X.R., Jian, Z.M., Su, X., 2006. A 33 Ma lithostratigraphic record of tectonic and paleoceanographic evolution of the South China Sea. Marine Geology 230 (3), 217–235.

Li, Z.L., Qiu, Z.L., Qin, S.C., Pang, X.B., Liang, D.H., Teng, Y.Y., Li, Y., 1991. A study on the forming conditions of basalts in seamounts of the South China Sea. Acta Mineralogy Sincia 11 (4), 325–333.

Li, P., Liang, H., 1994. Cenozoic magmatism in the Pearl river Mouth basin and its relationship to the basin evolution and petroleum accumulation. Guangdong Geology 9 (2), 23–34 (in Chinese with English abstract).

Pautot, G., Rangin, C., Briais, A., Wu, J.L., Han, S.Q., Li, H.X., Lu, Y.X., Zhao, J.C., 1990. The axial ridge of the south china sea-a seabeam and geophysical survey. Oceanologica Acta 13 (2), 129–143.

Renne, P.R., Mundil, R., Balco, G., Min, K., Ludwig, K.R., 2010. Joint determination of $^{40}K$ decay constants and $^{40}Ar^{*}/^{40}K$ for the Fish Canyon sanidine standard, and improved accuracy for $^{40}Ar/^{39}Ar$ geochronology. Geochimica et Cosmochimica Acta 74 (18), 5349–5367.

Renne, P.R., Balco, G., Ludwig, K.R., Mundil, R., Min, K., 2011. Response to the comment by W.H. Schwarz et al. on "Joint determination of K-40 decay constants and $^{40}Ar^{*}/^{40}K$ for the Fish Canyon sanidine standard, and improved accuracy for $^{40}Ar/^{39}Ar$ geochronology" by PR Renne, et al. (2010). Geochimica et Cosmochimica Acta 75 (17), 5097–5100.

Song, T.R., Li, C.F., 2012. The opening ages and mode of the South China Sea estimated from high-density magnetic tracks. Progress in Geophysics 27 (4), 1432–1442 (in Chinese with English abstract).

Taylor, B., Hayes, D.E., 1980. The tectonic evolution of the South China Basin. Geophysical Monograph Series 23, 89–104.

Taylor, B., Hayes, D.E., 1983. Origin and history of the South China Sea basin. Geophysical Monograph Series 27, 23–56.

Tu, K., Flower, M.F.J., Carlson, R.W., Xie, G.H., Chen, C.Y., Zhang, M., 1992. Magmatism in the South China Basin. 1. Isotopic and trace-element evidence for an Endogenous Dupal Mantle Component. Chemical Geology 97 (1), 47–63.

Wang, J.X., Wu, M.Q., Liang, D.H., Yin, A.W., 1984. Some geochemical characteristics of basalts in the South China Sea. Geochemica 4, 332–340.

Wang, P.X., 2012. Tracing the life history of a marginal Sea—on the "South China Sea Deep" Research Program. Chinese Science Bulletin 57 (20), 1807–1826.

Wang, Y.J., Han, X.Q., Luo, Z.H., Qiu, Z.Y., Ding, W.W., Li, J.B., Gao, S.T., Chen, R.H., 2009. Late Miocene magmatism and evolution of Zhenbei-Huangyan seamount in the South China Sea: evidence from petro-chemistry and chronology. Acta Oceanologica Sinica 31 (4), 93–102 (in Chinese with English abstract).

Wei, X., Zhu, Y.J., Chen, Y.H., Hu, G.L., Wu, J.Y., Jiang, J.Q., Li, Z.Y., 2012. Ocean crust character and spreading age of northwest sub-sea, the South China Sea: evidence from sediment strata and the abnormity of gravity and magnetism. Acta Geologica Sinica 86 (3), 383–388 (in Chinese with English abstract).

Xiao, L., Zhou, H.M., Dong, Y.X., Zeng, G.C., Wang, F.Z., 2006. Geochemistry and petrogenesis of Cenozoic volcanic rocks from Sanshui basin: impilications for spatial and temporal variation of rock types and contraints on the formation of South China Sea. Geotectonica et Metalogenia 30 (1), 72–81.

Xu, Y.G., Wei, J.X., Qiu, H.N., Zhang, H.H., Huang, X.L., 2012. Opening and evolution of the South China Sea constrained by studies on volcanic rocks: Preliminary results and a research design. Chinese Science Bulletin 57 (20), 1863–1878.

Yan, Q.S., Shi, X.F., Wang, K.S., Pu, W.R., Xiao, L., 2008. Study on major elements, trace elements and Sr-Nd-Pb isotopes of the Cenozoic alkali basalts, the South China Sea. Science in China (Series D) 38 (1), 56–71.

Yan, Q., Shi, X.F., Castillo, P.R., 2014. The late Mesozoic–Cenozoic tectonic evolution of the South China Sea: a petrologic perspective. Journal of Asian Earth Sciences 85 (0), 178–201.

Yang, S.Y., Fang, N.Q., Yang, S.X., Yao, B.C., Liang, D.H., 2011. A futher discussion on formation background and tectonic constraints of igneous rocks in central subbasin of the South China Sea. Earth Science (Journal of China University of Geosciences) 3 (4), 455–470.

Yao, B.C., 1998. Arguments of the sea floor spreading ages of South China Sea. Geological Research of South China Sea 10, 23–33 (in Chinese with English abstract).

Yao, B.C., 1999. Tectonic characteristics of Northwest sub-basin and seafloor spreading history of South China Sea in Cenozoic. Tropic Oceanology 18 (1), 7–15 (in Chinese with English abstract).

Yao, B.C., 1996. Tectonic evolution of the south China sea in Cenozoic. Marine Geology and Quaternary Geology 16 (2), 1–13 (in Chinese with English abstract).

Yao, B.C., 1997. The sea floor spreading in the SW sub-basin of South China Sea and it's tectonic significance. Geological Research of South China Sea 9, 20–36 (in Chinese with English abstract).

Zhang, T., Gao, J.Y., Li, J.B., Wu, Z.C., Wu, Z.L., Zhao, L.H., Yang, C.G., Shen, Z.Y., Zhou, Z.Y., 2012. The magnetic lineation identifications and segmentation of the northwestern sub-basin in the South China Sea. Chinese Journal of Geophysics 55 (9), 3163–3172 (in Chinese with English abstract).

Zhu, B.Q., Wang, H.F., 1989. Nd-Sr-Pb isotopic and chemical evidence for the volcanism with MORB-OIB source characteristics in the Leiqiong area, China. Geochemica 3, 193–201.

Zou, H.P., Li, P.L., Rao, C.T., 1995. Geochemistry of Cenozoic volcanic rocks in Zhu Jiangkou basin and its geodynamic significance. Geochemica 24, 33–45.